Haimovich, J., Eisen, H. N., Hurwitz, E., & Givol, D. (1972) *Biochemistry 11*, 2389–2398.
Hardy, R. R., & Richards, J. H. (1978) *Biochemistry 17*, 3866–3871.
Inbar, D., Hochman, J., & Givol, D. (1972) *Proc. Natl. Acad. Sci. U.S.A. 69*, 2659–2662.
Jackson, W. R. C., & Dwek, R. A. (1981) *Mol. Immunol. 18*, 499–506.
Jackson, W. R. C., Leatherbarrow, R. J., Gavish, M., Givol, D., & Dwek, R. A. (1981) *Biochemistry 20*, 2339–2345.
Kalk, A., & Berendsen, H. J. C. (1976) *J. Magn. Reson. 24*, 343–366.
Orin, G. B., Davis, R. C., Freed, R. M., & Rockey, J. M. (1976) *Immunochemistry 13*, 517–523.
Padlan, E. A., & Davies, D. R. (1975) *Proc. Natl. Acad. Sci. U.S.A. 72*, 819–823.
Padlan, E. A., Davies, D. R., Pecht, I., Givol, D., & Wright, C. E. (1976) *Cold Spring Harbor Symp. Quant. Biol. 41*, 627–637.
Perkins, S. J., & Dwek, R. A. (1980) *Biochemistry 19*, 245–258.
Perkins, S. J., Dower, S. K., Gettins, P., Wain-Hobson, S., & Dwek, R. A. (1977) *Biochem. J. 165*, 223–225.
Poljak, R. J., Amzel, L. M., Avey, H. P., Chen, B. L., Phizackerley, R. P., & Saul, F. (1973) *Proc. Natl. Acad. Sci. U.S.A. 70*, 3305–3310.
Poljak, R. J., Amzel, L. M., Chen, B. L., Phizackerley, R. P., & Saul, F. (1974) *Proc. Natl. Acad. Sci. U.S.A. 71*, 3440–3444.
Riordan, J. F., Sokolovsky, M., & Vallee, B. C. (1967) *Biochemistry 6*, 358–361.
Snyder, G. H., Rowan, R., Karplus, S., & Sykes, B. D. (1975) *Biochemistry 14*, 3765–3777.
Stanford, J. H., & Wu, T. T. (1981) *J. Theor. Biol. 88*, 421–439.
Vincent, J. P., Lazdunski, M., & Delaage, M. (1970) *Eur. J. Biochem. 12*, 250–257.
Wain-Hobson, S. (1977) D.Phil. Thesis, Oxford.

Nuclear Overhauser Assignment of the Imino Protons of the Acceptor Helix and the Ribothymidine Helix in the Nuclear Magnetic Resonance Spectrum of *Escherichia coli* Isoleucine Transfer Ribonucleic Acid: Evidence for Costacked Helices in Solution†

Dennis R. Hare‡ and Brian R. Reid*

ABSTRACT: In a previous study we showed that, in the low-field nuclear magnetic resonance (NMR) spectrum of *Escherichia coli* $tRNA_1^{Val}$, the hydrogen-bonded imino protons of the four Watson–Crick base pairs in the dihydrouridine helix could be assigned on the basis of their proximity to the imino proton of s^4U8 by means of sequential Nuclear Overhauser (NOE) connectivity (Hare & Reid, 1982). In the present paper we have used the nearest-neighbor NOE technique to assign all the imino proton resonances of the acceptor helix and the ribothymidine helix of *E. coli* $tRNA_1^{Ile}$. As reference points we used the GU-type base pairs located at positions 5 and 49 in this molecule which are readily identifiable in the NMR spectrum by virtue of containing two imino protons in the same base pair. From UG5 the imino protons of base pairs 4,3,2,1 and 6,7 could be assigned by through-space NOE connectivity. Similarly the imino protons of 50,51,52,53 were assigned by their spatial relationship to GΨ49. NOE connectivity also revealed a base pair stacked on the external side of GC53 which, by analogy with the crystal structure of yeast phenylalanine tRNA, is presumed to be the tertiary pair T54–A58. This was confirmed by NOE connectivity from the thymine methyl resonance. In addition to assigning 17 of the imino resonances in the low-field NMR spectrum of isoleucine tRNA, these NOE studies show that the acceptor helix and the ribothymidine helix are stacked on each other in solution in that base pairs 7 and 49 are directly connected in space.

One of the most useful applications of NMR is the ability of this technique to elucidate the three-dimensional folding of polymers from the spatial proximity of assigned resonances in the linear sequence via the nuclear Overhauser effect (NOE).[1] The NOE proximity technique makes use of the marked distance dependence of the negative NOE in polymers. If a given proton in a NMR spectrum is individually saturated by selective radio-frequency irradiation at its resonance frequency, its principal mode of recovery is by cross-relaxation with neighboring protons provided the correlation time is long compared to the reciprocal of the NMR frequency (this condition is met in large, slowly tumbling rigid polymers). A consequence of this cross-relaxation ("mutual spin flips") is that the neighboring protons become cross-saturated, and this is the basis of the negative NOE observed in polymers (Noggle

† From the Chemistry Department and Biochemistry Department, University of Washington, Seattle, Washington 98195. *Received May 4, 1982.* This work was supported by research grants from the National Science Foundation (PCM-8140603), the National Institute of General Medical Sciences (GM28764), and the American Cancer Society (N-P-191D) and by instrumentation grants from the Murdock Foundation, the National Science Foundation (PCM80-18053), and the National Institutes of Health (GM28764-01S1).

‡ D.R.H. is a predoctoral student in the graduate program of the Biochemistry Department, University of California, Riverside, CA 92521.

[1] Abbreviations: tRNA, transfer ribonucleic acid; NMR, nuclear magnetic resonance; NOE, nuclear Overhauser effect; DSS, 4,4-dimethylsilapentane-1-sulfonate; T, ribothymidine; D, dihydrouridine; Ψ, pseudouridine; EDTA, ethylenediaminetetraacetic acid.

0006-2960/82/0421-5129$01.25/0

& Schirmer, 1971; Bothner-By, 1979). The extent of cross-saturation of any particular neighbor depends exponentially on its proximity to the saturated proton (r^{-6}) and on the number of proximal protons in the immediate vicinity that are being simultaneously cross-saturated. This is the underlying process in the truncated driven NOE (TOE) technique which has been used for estimating relative proton–proton distances in proteins (Dubs et al., 1979; Wagner & Wuthrich, 1979; Poulsen et al., 1980). In general proton–proton NOEs are detectable only out to distances of around 4 Å, beyond which the effect falls to about 1% and becomes virtually undetectable.

In nucleic acids the extreme low-field part of the NMR spectrum contains one hydrogen-bonded imino proton from each complementary base pair and is the most resolved and informative region of the spectrum. When only the imino proton resonances of nucleic acids are considered, because of the separation between base pair planes, a given imino proton is usually at least 3.8 Å away from any other imino proton. The only time two imino protons can approach within 3 Å is when they are in the same base pair, i.e., a GU wobble pair. In such situations the G imino proton carries a large part of the U imino proton cross-relaxation, becoming heavily cross-saturated when it is irradiated and vice versa. Johnston & Redfield (1978, 1981) made use of this large (30–40%) negative imino–imino NOE to identify the two imino proton resonances of the GU4 wobble pair in yeast $tRNA^{Phe}$; Hurd & Reid (1979) subsequently used the same method to identify both of the imino protons of GU50 in the low-field NMR spectrum of *E. coli* $tRNA_1^{Val}$. Roy & Redfield (1981) have recently extended this technique to show that the GΨ pair in the D helix of yeast $tRNA^{Asp}$ also contains two hydrogen-bonded imino protons in wobble geometry.

Since, with signal averaging to high signal-to-noise levels, we were recently successful in observing the much weaker (2–4%) NOEs between the imino protons of adjacent Watson–Crick pairs in the D helix of *E. coli* $tRNA_1^{Val}$ (Hare & Reid, 1982), we reasoned that the four easily identifiable imino resonances from the two wobble pairs in *E. coli* $tRNA_1^{Ile}$ might be the best starting points from which to attempt to identify all the Watson–Crick pairs in the acceptor helix and ribothymidine (T) helix of this molecule by sequential NOE connectivity in space. The present communication assigns the imino protons of base pairs 4,3,2,1 and 6,7 by sequential NOE connectivity to UG5 in *E. coli* $tRNA^{Ile}$ and also assigns the imino protons of base pairs 50,51,52,53,54 by sequential NOE connectivity to GΨ49. Furthermore, our direct observation of a NOE between base pair 7 in the acceptor helix and base pair 49 in the ribothymidine helix establishes that these two helices are stacked upon each other in solution in $tRNA_1^{Ile}$ as predicted from the crystal structure of yeast $tRNA^{Phe}$.

Materials and Methods

E. coli B $tRNA_1^{Ile}$ was purified to homogeneity from unfractionated tRNA by chromatography on benzoylated DEAE-cellulose at pH 5.0 (Gillam et al., 1967) followed by chromatography on DEAE-Sephadex at pH 7.5 (Nishimura, 1971) and finally chromatography on Sepharose 4B (Holmes et al., 1975). On BD-cellulose the major peak of $tRNA_1^{Ile}$ elutes at approximately 0.92 M NaCl along with threonine and arginine tRNA, following $tRNA^{mMet}$ and preceding $tRNA_2^{Val}$. The second half of this material was pooled and chromatographed on DEAE-Sephadex from which it was the first tRNA species to elute from the column as a shoulder on the leading edge of the first major peak, before $tRNA_2^{Val}$, $tRNA^{Arg}$, and $tRNA^{Leu}$. The leading shoulder from DEAE-Sephadex was pooled and chromatographed on Sepharose 4B with a reverse ammonium sulfate gradient; the $tRNA_1^{Ile}$ eluted as a symmetrical pure peak at the beginning of the elution profile. The final pure $tRNA_1^{Ile}$ accepted 1800 pmol of isoleucine when aminoacylated with partially purified isoleucyl-tRNA synthetase.

Magnesium ion was removed from $tRNA_1^{Ile}$ by heating 12-mg samples in 10 mL of 10 mM EDTA at 50 °C for 10 min. The cooled solution was then vacuum dialyzed against 2 L of 10 mM sodium cacodylate, pH 7.2. When the sample volume reached 0.3–0.4 mL, it was transferred to a 5-mm Norell 505 NMR tube after addition of 0.05 volume of D_2O as a lock signal and DSS to a concentration of 0.2 mM as a chemical shift reference. For studies in the presence of Mg^{2+}, appropriate small volumes of 100 mM $MgCl_2$ were added to produce the desired final concentration of magnesium ion.

NMR spectra were collected on a Bruker WM500 FT NMR spectrometer. A modified Redfield 21412 pulse (Redfield & Kunz, 1979) was used to suppress the 110 M H_2O signal. A total pulse length of 0.205 ms was used with the carrier frequency placed 4730 Hz downfield of water. Transients were digitized to 16 bits resolution and accumulated in 8K channels of 24 bit memory. Reference spectra required about 400 pulses to achieve signal-to-noise ratios of 50. NOEs were observed by directly collecting the difference FID; this was accomplished by interleaving eight transients, after saturation of a given resonance, with eight transients of off-resonance irradiation, negating memory between the eight-transient cycles. Sufficient signal-to-noise was usually achieved in 4000–8000 transients to observe NOEs as small as 2%.

Results

The sequence of *E. coli* $tRNA_1^{Ile}$ (Yarus & Barrell, 1971) arranged in the standard two-dimensional cloverleaf folding pattern is shown in Figure 1, together with the low-field imino proton NMR spectrum of this molecule. Hydrogen-bonded imino protons generally occur between −15 ppm and −11 ppm, and partially inaccessible imino protons that are not hydrogen bonded usually resonate in the −11- to −9-ppm region (Reid, 1981). The spectrum in Figure 1 was obtained in the absence of magnesium ion, and there are 27 resolved peaks between −15 ppm and −11 ppm which are labeled A through W. Visual inspection reveals that all of the peaks have single proton intensity, indicating the presence of 27 long-lived imino hydrogen bonds. Upon addition of magnesium ion J′ moves downfield onto J, N′ moves downfield onto N, O′ moves downfield onto O, and F moves upfield toward G. These magnesium-induced shifts will be the subject of a later communication; most of the data in this report were obtained with magnesium-free samples.

Examination of the sequence of *E. coli* $tRNA_1^{Ile}$ reveals the presence of two potential wobble base pairs in the secondary structure, namely, UG5 and GΨ49. In order to test whether these both exist in solution as wobble base pairs, the size of the NOE to all other low-field resonances was monitored when each individual line between −14 ppm and −10 ppm was saturated. The data are presented in Figure 2 as difference spectra in which all unaffected lines cancel out, leaving only the large peak of the directly saturated resonance and smaller peaks for any cross-saturated resonances. Only two pairs of imino–imino NOEs of amplitude greater than 10% were observed, namely, S with X and U with W. Obviously the S,X pair is UG5 or GΨ49 in wobble geometry, and the U,W pair is either GΨ49 or UG5.

In order to distinguish which was which, we made use of the cloverleaf sequence and some empirical observations on the intra-base-pair NOE patterns of AU and GC pairs ob-

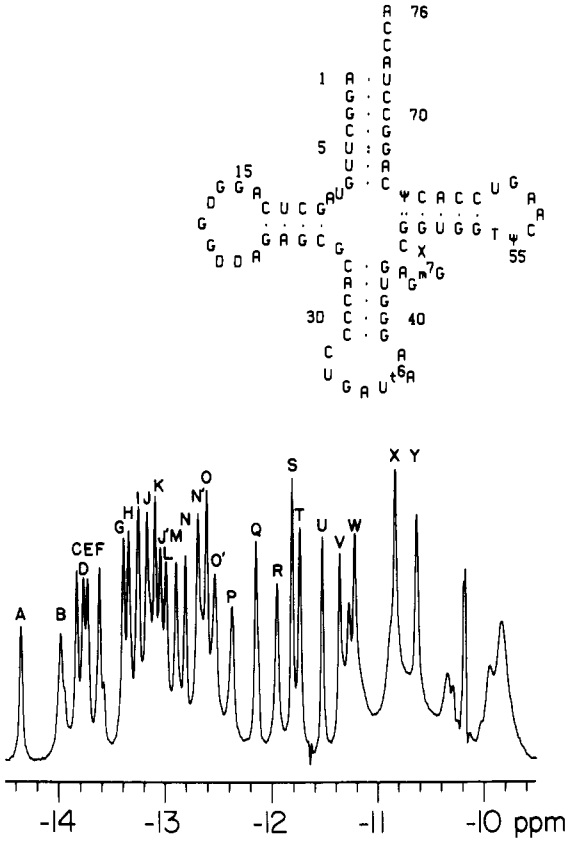

FIGURE 1: (Lower) 500-MHz low-field NMR spectrum of *E. coli* $tRNA_1^{Ile}$ at 32 °C in 10 mM sodium cacodylate, pH 7.0, after complete removal of magnesium ion. The resolved peaks referred to in the text are labeled alphabetically from A to Y. (Upper) The sequence of *E. coli* $tRNA_1^{Ile}$ arranged in the two-dimensional cloverleaf structure.

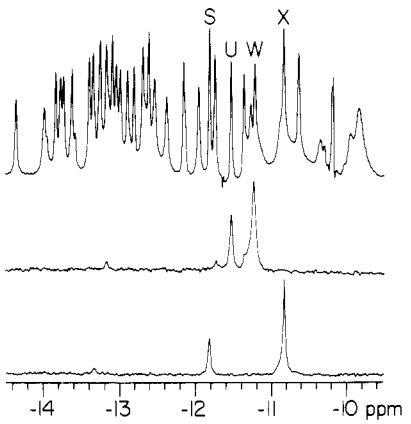

FIGURE 2: 500-MHz difference spectra showing the large imino–imino NOEs from peak X to peak S (bottom spectrum) and from peak W to peak U (middle spectrum) which identify the two wobble base pairs in *E. coli* $tRNA_1^{Ile}$.

tained during the systematic pinpoint saturation of all the low-field lines. The imino proton of an AU pair contains an adjacent carbon-bonded proton (the adenine C2-H) whereas there are only nitrogen-bonded amino protons adjacent to the imino proton in a GC pair. Adenine C2-H lines are quite narrow (Schmidt & Edelheit, 1981) whereas nitrogen protons are relatively broad due to relaxation by ^{14}N. Thus irradiation of an AU imino proton can easily be distinguished from saturation of a GC imino proton on the basis of the sharp C2-H NOE around −7 to −8 ppm (see Figure 3). Although imino protons from Hoogsteen AU pairs also give CH NOEs (to adenine C8-H), they can be distinguished from Watson–Crick AU pairs by C8 deuteration (Sanchez et al., 1980). Examples

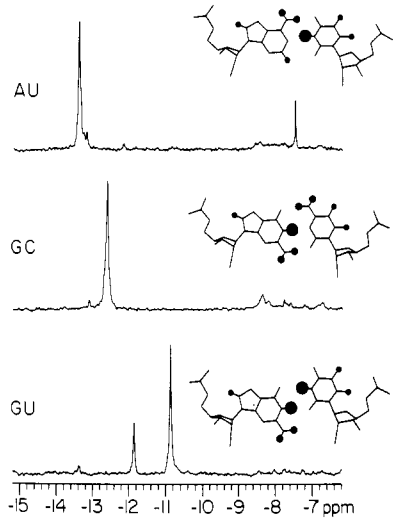

FIGURE 3: Characteristic *intra*-base-pair NOE patterns of AU, GC, and GU pairs. (Top) Irradiation of an AU imino proton cross-saturates a narrow line adenine C2-H as well as broad amino protons in the −6- to −9-ppm region. (Middle) Saturation of a GC imino proton produces NOEs only to broad amino protons in the −6- to −9-ppm region. (Bottom) Saturation of the G imino proton in a GU wobble pair strongly cross-saturates the U imino proton in the −10- to −15-ppm low-field spectrum. In the accompanying diagrams the imino protons are shown as large black circles, the amino protons as small black circles, and the carbon protons as gray concentric circles.

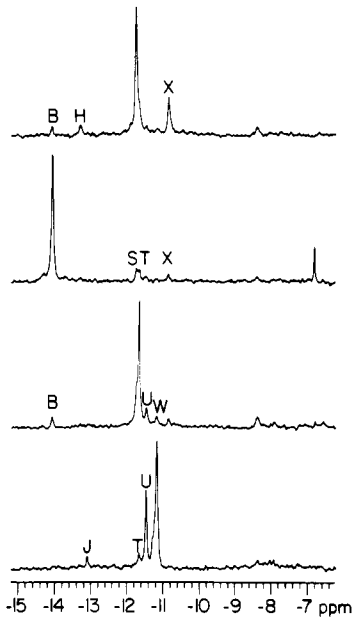

FIGURE 4: NOE connectivity from UG5 to GΨ49. (Top) Peak S strongly cross-saturates peak X and gives weaker NOEs to peaks B and H. (Second to top) Peak B gives weak NOEs to peak T as well as peaks S and X. The narrow C2-H NOE at −7 ppm indicates peak B is an AU pair. (Second to bottom) Peak T gives weak NOEs back to peak B and to peaks U and W (and X). (Bottom) Peak W heavily cross-saturates peak U and gives weak NOEs to peaks J and T.

of the intra-base-pair NOE patterns of AU, GC and GU pairs are shown in Figure 3. This characteristic behavior, combined with the sequence of *E. coli* $tRNA_1^{Ile}$, allowed us to assign the S,X and U,W resonances to their corresponding wobble pairs. GΨ49 has GC50 on one side and a potential GC7 on the other side, if the acceptor and T helices are stacked as in yeast $tRNA^{Phe}$. UG5, however, has UA6 and CG4 as nearest neighbors. The small nearest-neighbor imino NOEs from the S,X wobble pair shown in Figure 4 reveal that peaks B and H are its adjacent base pairs. Saturation of H indicates that

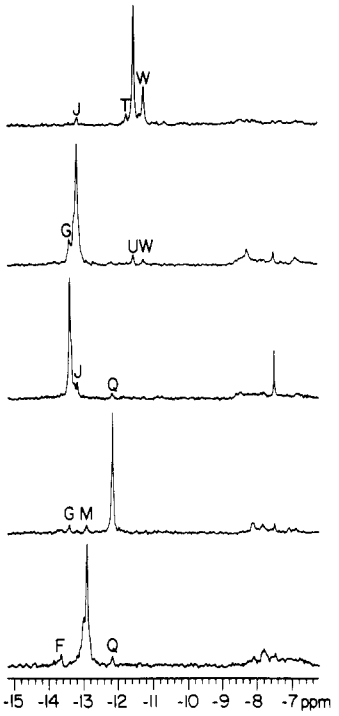

FIGURE 5: NOE connection from GΨ49 to GC53. (Top) Saturation of peak U (or W) gives NOEs back to peak T and on to peak J. (Second to top) Saturation of peak J reveals NOEs to peak G and to U,W. (Middle) Saturation of peak G gives NOEs to peaks J and Q. The narrow C2-H NOE at −7.6 ppm indicates peak G is an AU base pair. (Second to bottom) Peak Q gives NOEs back to peak G and also to peak M. (Bottom) Peak M is connected to both peak Q and peak F.

it is a GC pair, whereas saturation of peak B reveals a sharp C2-H NOE, indicating that it is an AU pair (see Figure 4). This immediately establishes that S,X is the UG5 wobble pair and that peaks H and B are CG4 and UA6, respectively. Further corroboration of this interpretation comes from the observation that the two neighbors of the U,W wobble pair (peaks J and T) are both GC pairs as expected for GΨ49 (see later).

With this foothold and orientation, saturation of peak B (UA6) revealed the expected NOE back to S,X and an additional NOE to peak T, which must be GC7 (Figure 4, second spectrum). If this interpretation is correct there are two predictions which now can be made. Saturation of peak T should not exhibit the AU-characteristic narrow C2-H NOE around −7 ppm and should show a weak nearest-neighbor NOE to the GΨ49 wobble pair (now assigned to the protons U and W) if the molecule folds in the same manner as does yeast $tRNA^{Phe}$. As shown in the third difference spectrum in Figure 4, both of these predictions are borne out. Saturation of T gives a NOE back to B and also cross-saturates the U,W pair. Furthermore, saturation of either U or W cross-saturates T and also reveals a NOE to a new UW neighbor, peak J. This series of spatial NOE connectivities now assigns peaks (S,X), B, T, and (U,W) to UG5, UA6, GC7, and GΨ49, respectively, and also assigns peak H to CG4 and peak J to GC50.

We next attempted to connect the resonances of the T helix starting at GΨ49 and working out toward the T loop. As shown in Figure 5, the U or W resonances of GΨ49 heavily cross-saturate each other and also give NOEs to peaks T and J. Peak J (GC50) in turn shows the expected reverse NOE back to U,W as well as a new NOE to peak G. Peaks G and J are separated by only 100 Hz, and the effect at G might, at first glance, be attributed to spillover of inadequately monochromatic irradiation of peak J. NOEs between resonances that are not well separated in the spectrum are a problem in this type of work; however, careful analysis of these spectra indicate that the effects are not due to spillover. For instance, irradiation of peak J produces a larger effect on peak G than on peak H, although peak H is closer to peak J and would be more affected by spillover. Similarly, in the reverse direction, peak J is more affected than is peak H by G irradiation, although peak H is the next peak to G in the spectrum. We therefore assign peak G to the imino proton of UA51. If this interpretation is correct, then saturation of peak G should give the narrow adenine C2-H NOE between −7 ppm and −8 ppm which is characteristic of AU pairs. As shown in the third spectrum of Figure 5, peak G is obviously an AU pair, corroborating our interpretation that it is UA51. Saturation of UA51 affected peak J and another nearest neighbor, namely, peak Q, which must be GC52. As seen in the fourth spectrum of Figure 5, irradiation of peak Q not only cross-saturates peak G as expected but also shows a new NOE to peak M which we assign to GC53. Saturation of peak M reveals a NOE to peak F as well as one back to peak Q. Although GC53 (peak M) is at the end of a secondary helix, the crystal structure of yeast $tRNA^{Phe}$ indicates that the tertiary base pairs T54–A58 and G18–Ψ55 are stacked on the end of the T helix. On the basis of this analogy we tentatively assigned peak F to the imino proton of T54–A58 and sought additional methods of corroborating this tertiary assignment.

Tropp & Redfield (1981) have carried out some elegant NOE studies on protons in the T loop of several tRNAs. Virtually all tRNAs contain ribothymidine as the first residue of the T loop, and the methyl protons of this residue resonate close to −1 ppm. They saturated the T methyl resonance and observed a NOE to an imino proton at around −11 ppm which was shown to be the Ψ55 N1-H by virtue of its coupling to the C6-H of Ψ55 (Tropp & Redfield, 1981). We decided to use a variation of this approach to try to assign the T54 imino proton from the "loop side". Although, according to the crystal structure, Ψ55 N1-H is only 3.5 Å from the T54 methyl group, the distance between the T54 imino proton and the T54 methyl group is 5.3 Å, and this is too far to observe a direct NOE. In order to traverse such a large distance, instead of using the TOE, we attempted to make use of the "domino effect" in spin diffusion whereby the protons affected by first-order NOEs can in turn cross-saturate their neighbors and spread the saturation further afield. Hence, we used an approximately steady-state approach in order to pick up these higher order NOEs. In this technique the T54 methyl protons were kept at least 65% saturated throughout the entire signal-averaging period. Experimentally the methyl resonance at −1 ppm was saturated for 0.8 s, and the saturating irradiation was only switched off during the acquisition (0.27 s) and "relaxation delay" (0.1 s) before the methyl signal was reirradiated; this 0.37 s of recovery is less than half of the T1 of the methyl protons, thus allowing the entire environment to approach steady-state cross-saturation while pumping only the methyl protons. The results are shown in the bottom spectrum of Figure 6. In addition to the large NOE to Ψ55 N1-H at −10.7 ppm (peak Y), we also observe weaker NOEs to peaks F, M, Q, and V. Peaks M and Q are already assigned to GC53 and GC52 based on their connectivity to GΨ49, and peak F is tentatively assigned to T54–A58. The relative orientation of all of these imino protons with respect to the T54 methyl group in the crystal structure is shown in Figure 7. The observation of saturation effects on base pairs 52 and 53 (approximately

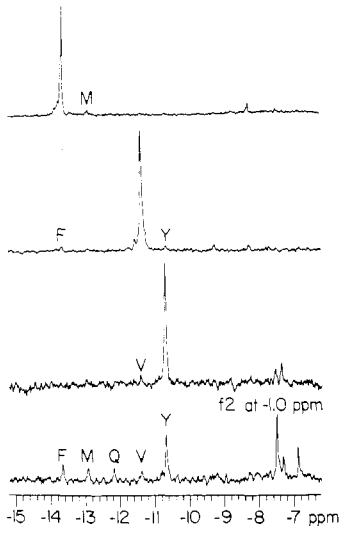

FIGURE 6: NOE connectivities from the T54 methyl resonance to the GC53 imino proton. (Bottom) Irradiation of the thymine methyl protons (−1 ppm) produces a large NOE to peak Y and smaller NOEs to peaks F, M, Q, and V. (Second to bottom) Saturation of peak Y (Ψ55 N1-H) produces a weak NOE at peak V (Ψ55 N3-H). (Second to top) Irradiation of peak V weakly cross-saturates peak F. (Top) Saturation of peak F gives a weak NOE to peak M (GC53) and a very weak NOE back to peak V.

6–7 Å away) indicates extensive spin diffusion (Kalk & Berendsen, 1976; Dubs et al., 1979). As shown in the second bottom spectrum of Figure 6, saturation of Ψ55 N1-H (peak Y) produces a very weak NOE to peak V at −11.4 ppm for which the most likely candidate is Ψ55 N3-H. Saturation of peak V cross-saturates peak F. Irradiation of peak F produces a weak NOE to peak M which we have already assigned to GC53. To further verify the spatial proximity of peaks M and F, we repeated the experiment in the presence of magnesium ion which increased this NOE somewhat. As shown in Figure 8, saturation of peak M (GC53) establishes without doubt that its neighbors are peaks Q and F. Thus we have spatially connected peak F from two different directions, namely, J-G-Q-M-F and Y-V-F-M; from its spatial location between GC53 and Ψ55, peak F can only be the imino proton of T54.

Going back to the assignment of UG5 (S,X) and CG4 (H), we next attempted to assign the remaining base pairs at the top of the acceptor helix. The effects of saturating peak H (CG4) are shown in Figure 9. The expected reverse NOE back to S,X is seen, and at first glance, there appears to be no other imino NOE. However, this anomaly turned out to be an extreme case of the situation in which two adjacent base pairs have very similar chemical shifts. Careful irradiation of peak H at various positions on the downfield side of the center of this peak revealed that there is a small NOE to peak I over and above the direct irradiation of I due to nonselectivity. Similar experiments on peak I revealed a weak NOE back to peak H, i.e., the effects on H are greater than simple spillover. An example is shown in Figure 10. Although peak J is 7 Hz closer to peak I than is peak H, it is less affected than peak H by irradiation centered on peak I, indicating that the greater effect on H is a bona fide NOE. Thus peaks H and I are not only close in frequency but are also dipolar coupled by spatial proximity and must be nearest neighbors. This then assigns peak I to GC3. Saturation of peak I produces a NOE to peak N which is GC2. Peak N shows NOEs to peaks I and E, and we assign peak E at −13.7 ppm to AU1. Saturation of peak E only produces one NOE back to peak N, as expected for a terminal base pair, and the chemical shift of peak E is highly indicative of an AU pair rather than a GC pair. However, unlike UA6 and UA51, AU1 produces only a relatively weak C2-H NOE in the aromatic carbon proton spectral region; this indicates a somewhat greater than usual distance between U72 N3-H and A1 C2-H and is presumably a reflection of the lowered stability of terminal base pairs.

Discussion

The results presented here show the feasibility of directly assigning the hydrogen-bonded imino proton resonances of adjacent base pairs in nucleic acids by through-space one-dimensional NOE connectivity. This has been previously accomplished only in the case of the four base-pair D helix of yeast $tRNA^{Asp}$ which contains two wobble pairs (Roy & Redfield, 1981) and the D helix of *E. coli* $tRNA_1^{Val}$ which contains four Watson–Crick pairs (Hare & Reid, 1982). Although the imino–imino proton distances are around 4 Å and the size of the NOEs is only a few percent, they are nevertheless unambiguously demonstrable with highly sensitive state-of-the-art instrumentation. Within a given helix these linear connectivities can be extended ad infinitum and, in favorable circumstances, can even connect one helix to another. In the present paper we were able to show the spatial connectivity between base pair 7 at the bottom of the acceptor helix and base pair 49 at the top of the T helix. Thus we have

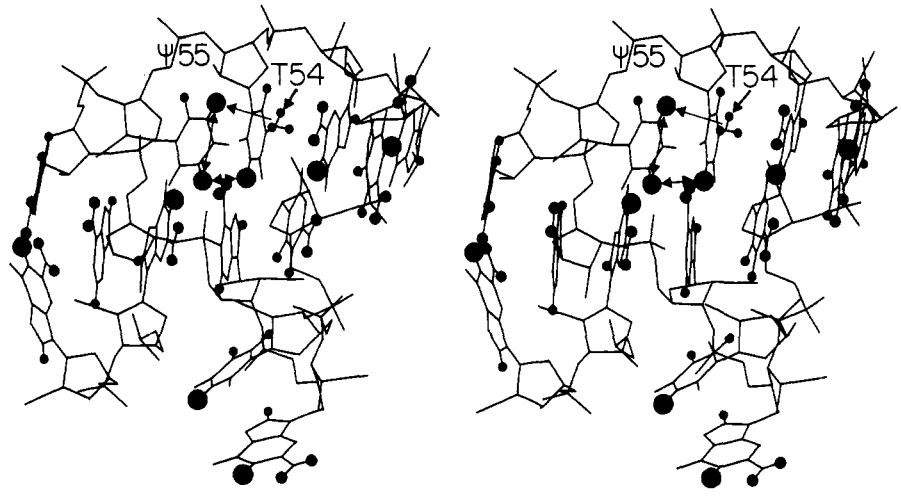

FIGURE 7: Stereo diagram of the T54–A58 and G18–Ψ55 tertiary base pairs at the end of the T helix. Imino protons are shown as large black circles, amino protons as small black circles, and carbon protons as gray concentric circles. The NOE connectivity path from the thymine methyl protons to imino resonances Y, V, and F is shown by arrows.

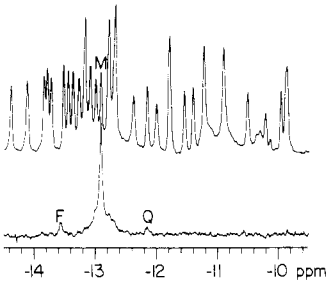

FIGURE 8: NOE from peak M to peaks F and Q in the presence of 10 mM magnesium ion.

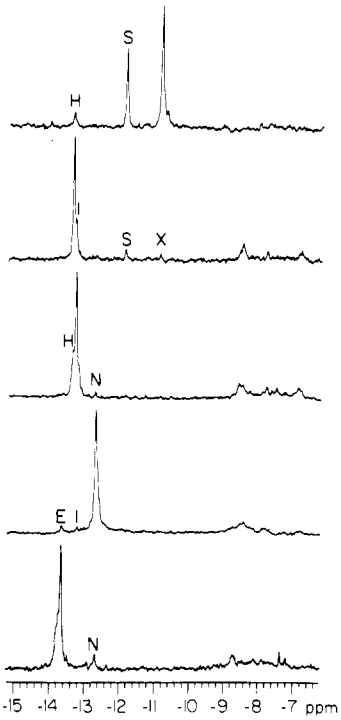

FIGURE 9: NOE connectivities (top to bottom) from peaks H to I, from peaks I to N, and from peaks N to E. The only NOE from peak E (AU1) is back to peak N (GC2).

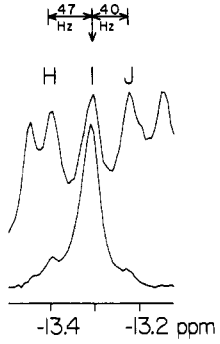

FIGURE 10: Expanded view of the H,I,J spectral region following 0.8-s irradiation of peak I. The effect on peak H is greater than the effect on peak J, although peak H is 7 Hz further away from peak I. Apart from peak N, there are no other observed imino NOEs from peak I.

established that, in solution as well as in the crystal structure, these two helices are juxtaposed by stacking upon each other. This result led to a linear chain of connectivity between base pair 1 at the top of the acceptor helix and tertiary base pair T54–A58 in the T loop, i.e., the complete top arm of the L-shaped three-dimensional structure. The crystallographic orientation of these 13 contiguous base pairs and their imino protons are shown in Figure 11; this connectivity chain traverses a distance of about 36 Å.

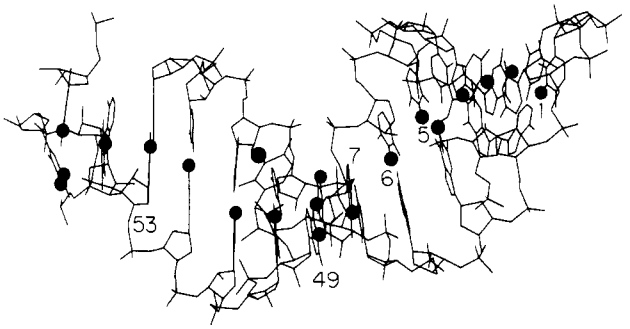

FIGURE 11: Computer drawing of the costacked acceptor helix (base pairs 1–7) and T helix (base pairs 49–53) according to the X-ray coordinates. Tertiary base pairs T54–A58 and G18–Ψ55 are shown on the left at the end of the T helix, and residue 8 is shown above base pair 50 to show the sharp turn in the backbone at position 8 which allows base pair 49 to stack on base pair 7. The backbone coordinates of yeast $tRNA^{Phe}$ were used (Sussman et al., 1978), and bases were replaced according to the $tRNA_1^{Ile}$ sequence. The imino protons responsible for the low-field NMR peaks are shown as black circles.

With suitable markers in the D helix and the anticodon helix, it should be possible to assign the imino protons from the other arm of the tRNA structure, thus identifying every resonance in the low-field spectrum by spatial connectivity. We are currently pursuing this goal in $tRNA_1^{Ile}$ and in other tRNA species. These assignments should prove to be of great value in examining the dynamics and interactions of tRNA in solution.

Acknowledgments

Thanks are due to Susan Ribeiro for purifying the *E. coli* $tRNA_1^{Ile}$. We also thank Gary Drobny for advice and assistance in NMR instrumentation and Alvin Kwiram for encouragement.

References

Bothner-By, A. A. (1979) in *Biological Applications of Magnetic Resonance* (Shulman, R. G., Ed.) p 177, Academic Press, New York.

Dubs, A., Wagner, G., & Wuthrich, K. (1979) *Biochim. Biophys. Acta 577*, 177.

Gillam, I., Millward, S., Blew, D., Von Tigerstrom, M., Wimmer, E., & Tener, G. M. (1967) *Biochemistry 6*, 3043.

Hare, D. R., & Reid, B. R. (1982) *Biochemistry 21*, 1835.

Holmes, W. M., Hurd, R. E., Reid, B. R., Rimerman, R. A., & Hatfield, G. W. (1975) *Proc. Natl. Acad. Sci. U.S.A. 72*, 1068.

Hurd, R. E., & Reid, B. R. (1979) *Biochemistry 18*, 4017.

Johnston, P. D., & Redfield, A. G. (1978) *Nucleic Acids Res. 5*, 3913.

Johnston, P. D., & Redfield, A. G. (1981) *Biochemistry 20*, 1147.

Kalk, A., & Berendsen, H. J. C. (1976) *J. Magn. Reson. 24*, 343.

Nishimura, S. (1971) in *Procedures in Nucleic Acid Research* (Cantoni, G. L., & Davies, D. R., Eds.) Vol. 2, p 542, Harper and Row, New York.

Noggle, J. H., & Schirmer, R. E. (1971) *The Nuclear Overhauser Effect: Chemical Applications*, Academic Press, New York.

Poulsen, F. M., Hoch, J. C., & Dobson, C. M. (1980) *Biochemistry 19*, 2597.

Redfield, A. G., & Kunz, S. D. (1979) in *NMR and Biochemistry* (Opella, S. J., & Lu, P., Eds.) p 225, Marcel Dekker, New York.

Reid, B. R. (1981) *Annu. Rev. Biochem. 50*, 969.
Roy, S., & Redfield, A. G. (1981) *Nucleic Acids Res. 9*, 7073.
Sanchez, V., Redfield, A. G., Johnston, P. D., & Tropp, J. (1980) *Proc Natl. Acad. Sci. U.S.A. 77*, 5659.
Schmidt, P. G., & Edelheit, E. B. (1981) *Biochemistry 20*, 79.
Sussman, J. L., Holbrook, S. R., Warrant, R. W., Church, G. M., & Kim, S. H. (1978) *J. Mol. Biol. 123*, 607.
Tropp, J., & Redfield, A. G. (1981) *Biochemistry 20*, 2133.
Wagner, G., & Wuthrich, K. (1979) *J. Magn. Reson. 33*, 675.
Yarus, M., & Barrell, B. G. (1971) *Biochem. Biophys. Res. Commun. 43*, 729–734.

Fluorescence Energy Transfer Studies of Skeletal Troponin C Proximity between Methionine-25 and Cysteine-98†

Herbert C. Cheung,* Chien-Kao Wang, and Frank Garland

ABSTRACT: The distance between two specific residues in skeletal troponin C was measured by the method of fluorescence energy transfer. Dansylaziridine attached to Met-25 was used as the energy donor and 5-(iodoacetamido)eosin attached to Cys-98 as the acceptor. The transfer efficiency was determined from quenching of donor intensity. An efficiency of 66% was obtained for Ca^{2+}-free troponin C and 81% for the fully saturated Ca^{2+} complex. From these results and depolarization data obtained from donor- and acceptor-labeled proteins, a range of the donor–acceptor distance (R) was calculated by the dynamic averaging method [Dale, R. E., Eisinger, J., & Blumberg, W. E. (1979) *Biophys. J. 26*, 161]. The ranges were 29–51, 26–51, and 26–51 Å for Ca^{2+}-free troponin C, the half-saturated Ca^{2+} complex, and fully saturated Ca^{2+} complex, respectively. These results suggest that Ca^{2+} binding may induce a very small reduction in the minimum donor–acceptor distance but does not produce any global deformation of troponin C. Qualitatively similar conclusions were obtained with 5-(iodoacetamido)fluorescein attached to Cys-98 as the acceptor. A rotational correlation time of 6.3 ns was determined by the nanosecond method for Ca^{2+}-free troponin C which was labeled with *N*-(iodoacetyl)-*N'*-(1-sulfo-5-naphthyl)ethylenediamine at Cys-98. While a reduction of about 1 ns in the correlation time was observed for the Ca^{2+} complexes, the change was too small to warrant any conclusion of a change in the overall shape of the protein induced by Ca^{2+} binding. The relatively large minimum distance between donor and acceptor sites suggests that structural perturbations initiated by Ca^{2+} binding to the high-affinity sites would be transmitted over a considerable distance to the attached donor probe.

While the molecular mechanism by which Ca^{2+} binding to troponin modulates actomyosin ATPase has not been fully elucidated, it is generally accepted that the binding triggers a series of reversible molecular changes which are propagated across the thin filament structure. The transfer of this structural information to specific sites on the actin filament results in the activation of the actin–myosin interaction. Since the stoichiometry of troponin:tropomyosin:actin is 1:1:7, the transfer of structural information which is induced by Ca^{2+} binding must occur over a large distance. Our present understanding of the transfer mechanism is poor because of the lack of detailed structural information.

Of the three subunits of troponin, TNC[1] is the Ca^{2+} receptor. The other two subunits, troponin T and troponin I, provide a link to tropomyosin and actin, and together they are thought to exert the inhibitory effect via tropomyosin on the actin–myosin interaction. The four Ca^{2+} binding sites of TNC can be divided into two classes according to their affinity for Ca^{2+}. The two low-affinity sites (sites 1 and 2) are Ca^{2+} specific, and the two high-affinity sites (sites 3 and 4) also bind Mg^{2+} competitively. The affinity of the two classes of sites for Ca^{2+} differs by about 2 orders of magnitude, with the affinity of the Ca^{2+} specific sites being about 3×10^5 M^{-1} (Potter & Gergely, 1975).

The three-dimensional structure of rabbit skeletal TNC has not yet been determined, although its amino acid sequence has been known for some time (Collins et al., 1977). By analogy with the primary structure of a parvalbumin, four homologous regions have been postulated as the Ca^{2+} binding sites of TNC (Kretsinger & Barry, 1975). Subsequent studies including those with cyanogen bromide and proteolytic fragments (Potter et al., 1976; Leavis et al., 1978) have established that the two regions corresponding to the Ca^{2+}-specific sites are located in the N-terminal half of the molecule and the other two regions corresponding to the Ca^{2+}–Mg^{2+} high-affinity sites are at the C-terminal half. Many spectroscopic studies have shown that Ca^{2+} binding to the high-affinity Ca^{2+}–Mg^{2+} sites produces large conformational changes in the C-terminal half of the molecule, as reflected by an increase in tyrosyl fluorescence (van Eerd & Kawasaki, 1972) and α helicity (Kawasaki & van Eerd, 1972), spectral shifts in the UV absorption curve (Head & Perry, 1974), and an enhancement of the fluorescence of extrinsic probes attached to Cys-98 (Potter et al.,

† From the Biophysics Section, Department of Biomathematics, University of Alabama in Birmingham, Birmingham, Alabama 35294.
Received December 22, 1981; revised manuscript received July 7, 1982. This work was supported in part by U.S. Public Health Service Grant AM-25193.

[1] Abbreviations: TNC, Ca^{2+} binding subunit of troponin; TNT, tropomyosin binding subunit of troponin; TNI, ATPase inhibitory subunit of troponin; DNZ, dansylaziridine; IAE, 5-(iodoacetamido)eosin; IAF, 5-(iodoacetamido)fluorescein; IAEDANS, *N*-(iodoacetyl)-*N'*-(1-sulfo-5-naphthyl)ethylenediamine; EGTA, ethylene glycol bis(β-aminoethyl ether)-*N*,*N*,*N'*,*N'*-tetraacetic acid; Tris, tris(hydroxymethyl)aminomethane; TNC-DNZ, TNC labeled with DNZ; TNC-IAE, TNC labeled with IAE; TNC-IAF, TNC labeled with IAF; TNC-DNZ-IAE, TNC doubly labeled with DNZ and IAE; TNC-DNZ-IAF, TNC doubly labeled with DNZ and IAF; DTNB, 5,5'-dithiobis(2-nitrobenzoic acid); DTT, dithiothreitol.

0006-2960/82/0421-5135$01.25/0